Supporting Information

A Comparative Study of Metal (Ni, Co, or Mn)-Borate Catalysts and Their Photodeposition on rGO/ZnO Nanoarrays for Photoelectrochemical Water Splitting

Huayang Zhang,[‡ab] Wenjie Tian,[‡a] Yunguo Li,[‡c] Hongqi Sun,*[b] Moses O. Tadé[a] and Shaobin Wang*[a]

[a] *WA School of Mines: Minerals, Energy and Chemical Engineering, Curtin University, GPO Box U1987, WA 6845, Australia. E-mail: shaobin.wang@curtin.edu.au*

[b] *School of Engineering, Edith Cowan University, 270 Joondalup Drive, Joondalup, WA 6027, Australia. E-mail: h.sun@ecu.edu.au*

[c] *Department of Earth Sciences, University College London, Gower Street, London WC1E 6BT, United Kingdom.*

‡ These a*uthors contributed equally.*

1. Simulation details

We performed spin-polarized DFT calculations in order to elucidate the OER activities of M-Bi (M = Ni, Co, Mn). We used the Vienna *Ab initio* Simulations Package (VASP)[1,2] and projected augmented wave (PAW)[3–5] method for total energy calculations. In the calculations, 3*d* and 4*s* electrons were treated as valence electrons for Ni, Co and Mn, and 2*s* and 2*p* for O. The exchange-correlation interaction was treated with Generalized gradient approximation (GGA) parameterized by Perdew, Burke and Ernzerhof (PBE).[6] For strongly localized *d* electrons, the GGA has systematic and noncancelling errors.[7] So, we adopted GGA+U[8] to correct the self-interaction error and overdelocalized *d* states. The effective U_{eff} introduced by Dudarev et al.[8] was used with 5.25, 4.5 and 5.5 eV for Ni,[8] Co,[9] and Mn,[10] respectively.

We started from relaxing bulk MO_2 (space group $R\bar{3}m$, No. 166) composed of MO_6 octahedra. The cutoff energy of plane-wave basis was set to 520 eV, and integrations over the first Brillouin zone were made using Gamma-centred k-point sets of 8×8×8. With these settings, the total energy was able to converge within 1 meV/atom. Atomic positions were fully relaxed with the energy converged within 10^{-6} eV/cell and the force converged to less than 10^{-4} eV/Å. Then, we relaxed the (100) surface with a single layer of MO_6 octahedra spaced by 17 Å. The (101)

zigzag ribbons were also relaxed in slab calculations. The same cutoff energy and similar k-point grids as dense as in the bulk calculations (in the case of vacuum direction, only Gamma point was used) were used for slab calculations. The detailed treatment of OER free energy calculations can be found in our previous publication.[11]

2. Materials characterizations

X-ray diffraction spectra were recorded on an Empyrean multi-purpose research diffractometer (Panalytical Empyrean XRD) using the filtered Cu Kα radiation (λ = 1.5418 Å) with an accelerating voltage of 40 kV and a current of 40 mA. The transmission electron microscopy (TEM) images were obtained on a JEOL 2100 TEM microscope (120 kV) and FEI TITAN G2 (200 kV). The high angle annular dark field scanning transmission electron microscopy (HAADF-STEM) images and EDX mapping analysis were carried out on FEI TITAN G2 (200 kV). X-ray photoelectron spectroscopy (XPS) was conducted under ultrahigh vacuum condition on a Kratos Axis Ultra DLD system. UV-visible diffuse reflectance spectra were collected on a Cary 100 UV-visible spectrophotometer (Agilent, US).

3. Real-time oxygen measurements

An oxygen sensor (Ocean Optics, Neofox, FOSPOR-R 1/16) was inserted into the photoelectrolytic glass cell to probe the produced O_2 concentration via the fluorescence quenching method during the stability test. The glass cell has a quartz window (the volume of the headspace was 30 mL, excluding the space occupied by the septum, oxygen sensor, and the solution). The needle probe was inserted into the 1/16" threaded holes through a rubber septum and conducted uninterrupted O_2 readings at 5 s intervals throughout the test. Ahead of the detection, the probe was calibrated through a 2-point method, with a reading error of 1%. Before irradiation, the reactor was purged with N_2 for 10 min to exclude air in the reaction system. The test started from 10 min baseline reading followed by 100 min irradiation under AM 1.5G simulated solar light (light intensity: 1 sun or 100 mW cm^{-2}) with the potentiostatic method (at 1.23 V vs. RHE).

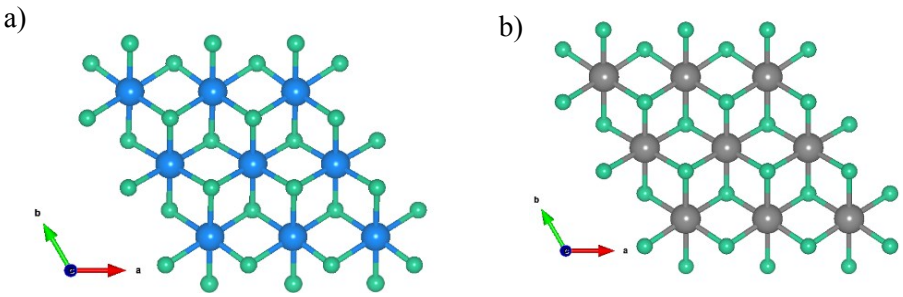

Fig. S1 Model structures for a) CoO_6 and b) MnO_6.

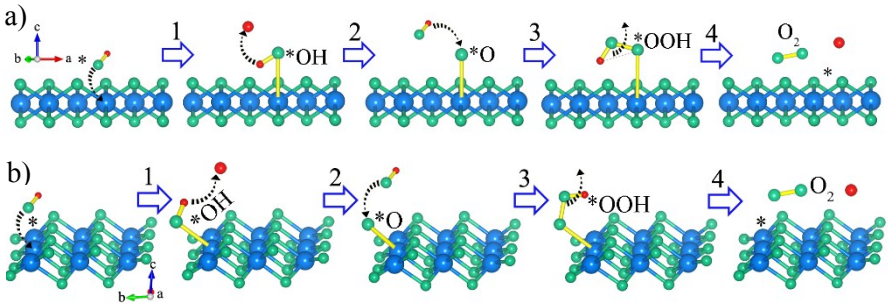

Fig. S2 Proposed 4-step OER paths with *OH, *O and *OOH adsorbed on selected Co sites at a) (001) surface and b) (101) surface of CoO_6 (pH = 9.2).

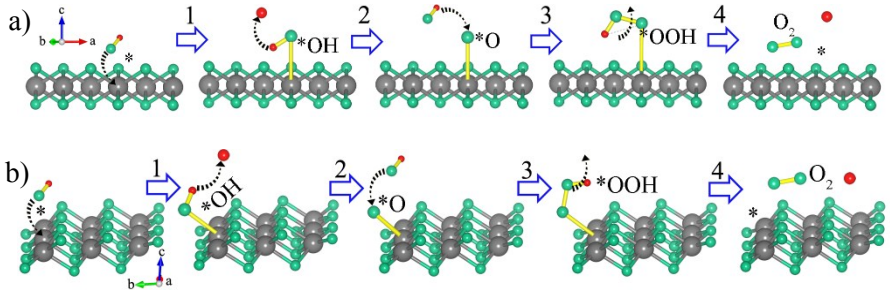

Fig. S3 Proposed 4-step OER paths with *OH, *O and *OOH adsorbed on selected Co sites at a) (001) surface and b) (101) surface of MnO_6 (pH = 9.2).

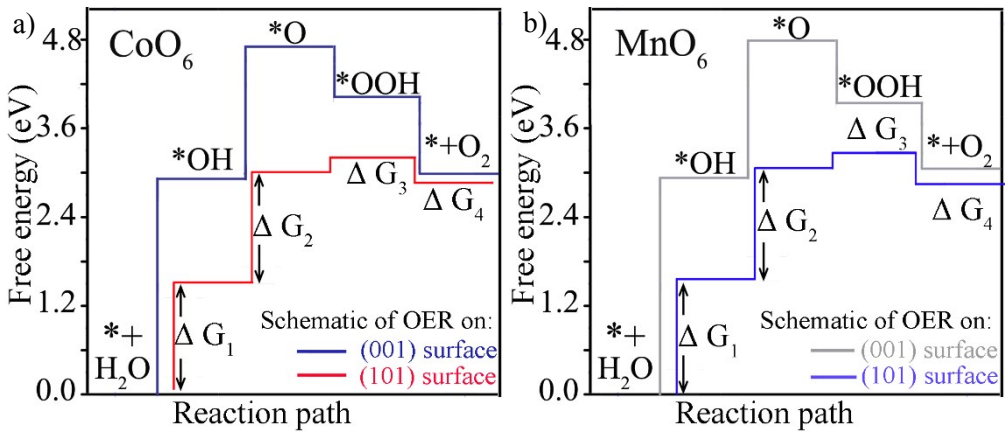

Fig. S4 Diagrams of the 4-step Gibbs free energy changes calculated on the (001) surface and (101) surface in a) CoO_6 and b) MnO_6.

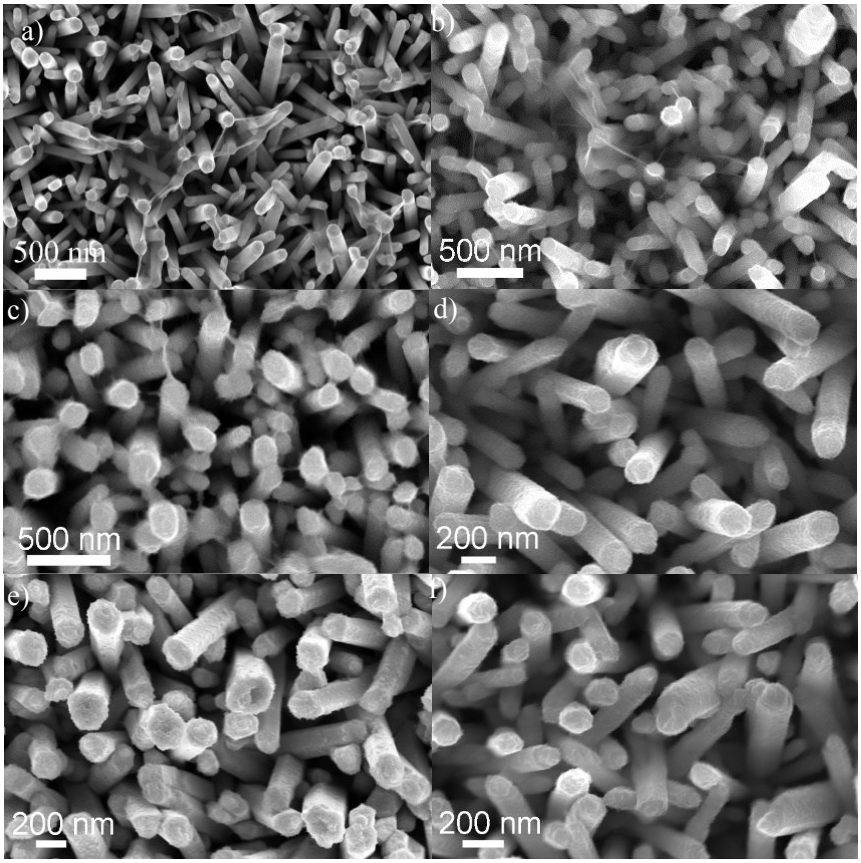

Fig. S5 SEM images of a) rGO/ZnO, b) Co-Bi/rGO/ZnO, c) Mn-Bi/rGO/ZnO, d) Ni-Bi/ZnO, e) Co-Bi/ZnO and f) Mn-Bi/ZnO.

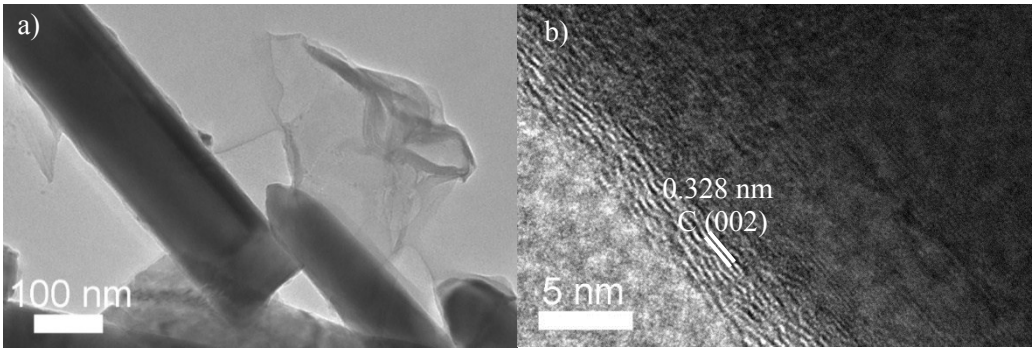

Fig. S6 a) TEM and b) HRTEM images of rGO/ZnO.

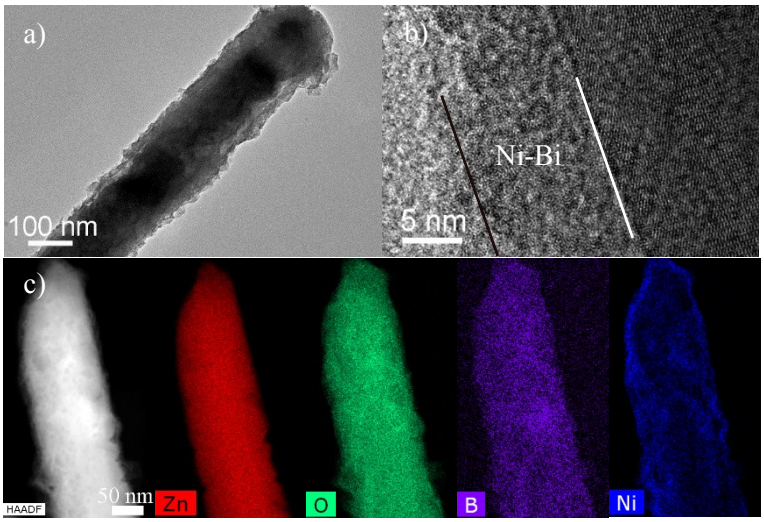

Fig. S7 a) TEM, b) HRTEM and c) HAADF-STEM with EDX mapping images of Ni-Bi/ZnO.

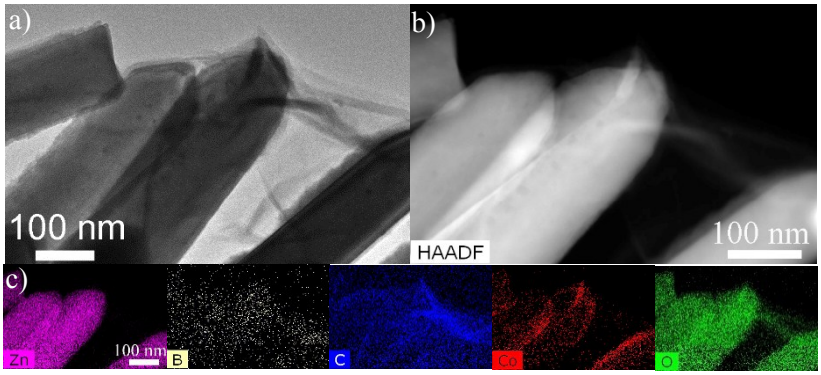

Fig. S8 a) TEM, b) HAADF-STEM and c) EDX mapping images of Co-Bi/rGO/ZnO.

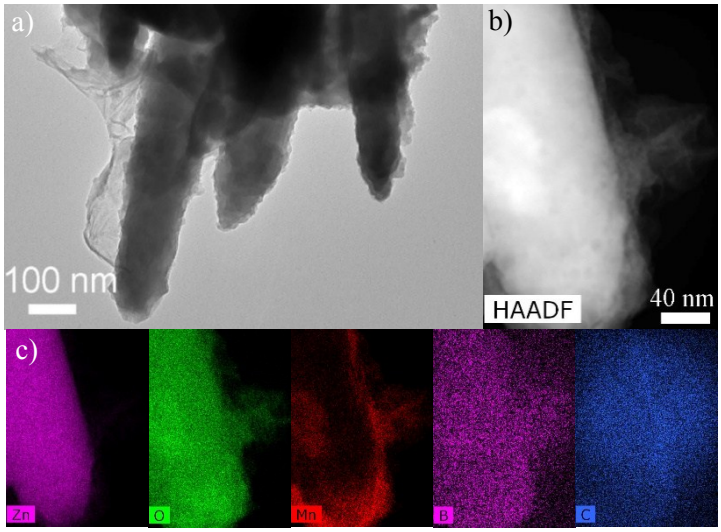

Fig. S9 a) TEM, b) HAADF-STEM and c) EDX mapping images of Mn-Bi/rGO/ZnO.

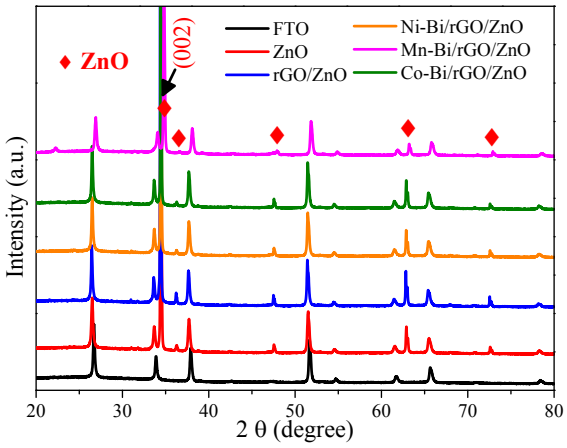

Fig. S10 XRD patterns of FTO substrate, ZnO, rGO/ZnO and M-Bi/rGO/ZnO.

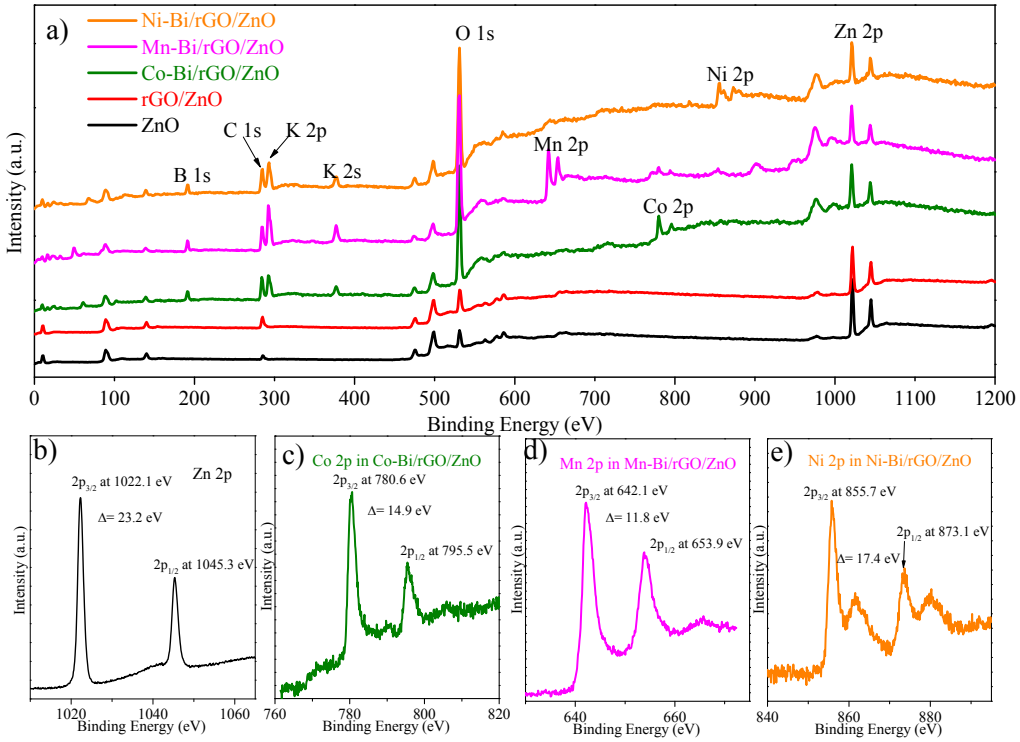

Fig. S11 a) Full XPS spectra of the samples and high-resolution spectra of b) Zn 2p, c) Co 2p, d) Mn 2p and e) Ni 2p.

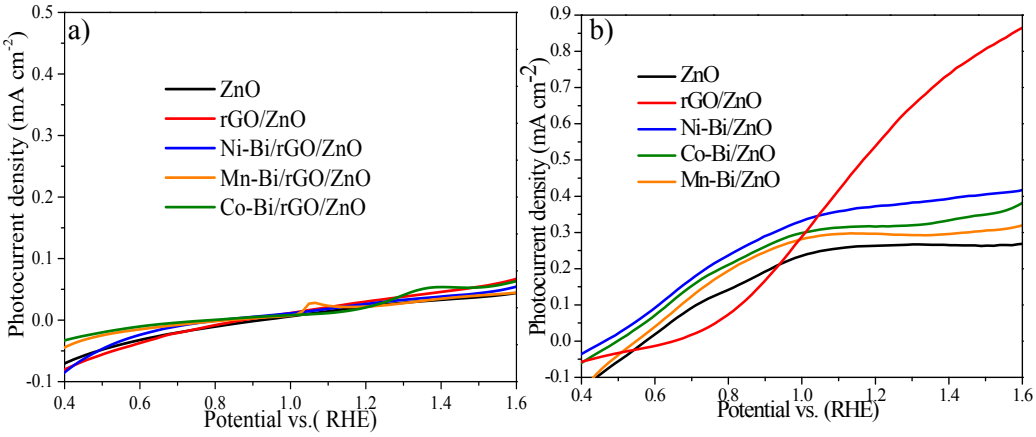

Fig. S12 J-V curves tested on ZnO, rGO/ZnO, and M-Bi/ZnO under a) dark condition and b) irradiation.

In dark condition (Fig. S12a), the small peaks observed on Mn-Bi/rGO/ZnO (at 1.05 V) and Co-Bi/rGO/ZnO (at 1.4 V) were caused by the valence state changes of Mn and Co species due to the oxidation.[12,13]

Table S1. A comparison of the PEC performance of Ni-Bi/rGO/ZnO with previously reported ZnO-based catalysts for water oxidation in a mild medium under light intensity of 100 mW cm^{-2}.

Photoanode	Photocurrent density (potentials vs. RHE)	Testing condition	Reference
C-doped ZnO	1.00 mA cm^{-2} at 1.61 V	0.5 M Na_2SO_4	14
Au NP/$ZnFe_2O_4$/ZnO	1.1 mA cm^{-2} at 1.4 V	0.5 M Na_2SO_4	15
3D ZnO/TiO_2/FeOOH NWs	1.59 mA cm^{-2} at 1.8 V	0.5 M Na_2SO_4	16
$Ni(OH)_2$/ZnO NR	~0.90 mA cm^{-2} at 1.2 V	0.5 M Na_2SO_4	17
Au-ZnO nanopencil	~1.5 mA cm^{-2} at 1.6 V	0.5 M Na_2SO_4	18
ZnO-Au-SnO_2 nanorods	0.08 mA cm^{-2} at 1.4 V	0.5 M Na_2SO_4	19
(N-GQDs)/ZnO nanowire	~0.6 mA cm^{-2} at 1.63 V	0.5 M Na_2SO_4	20
CdS/RGO/ZnO Nanowire	0.8 mA cm^{-2} at 1.63 V	0.1 M phosphate buffer solution	21
Three-dimensional ZnO nanoforests	0.919 mA cm^{-2} at 1.81 V	0.5 M Na_2SO_4	22
Au-ZnO Nanowire	1.3 mA cm^{-2} at 1.6 V	0.5 M Na_2SO_4	23
ZnO-IrOx nanorod	0.7 mA cm^{-2} at 1.2 V	0.25M Na_2SO_4	24
Ni-Bi/rGO/ZnO	1.15 mA cm^{-2} at 1.6 V	0.2 M K-Bi	This work

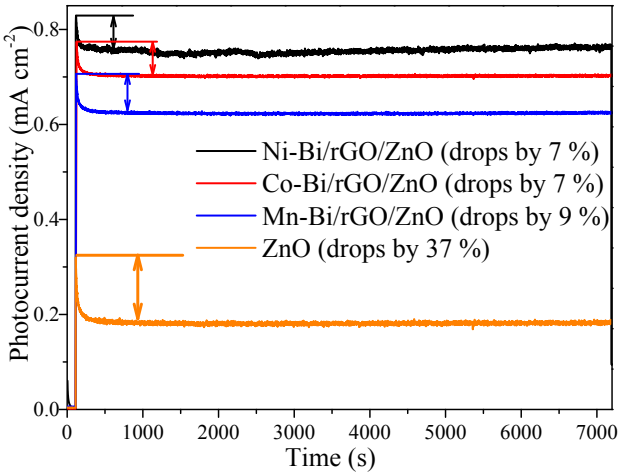

Fig. S13 Potentiostatic measurements (at 1.23 V vs RHE) of ZnO and M-Bi/rGO/ZnO.

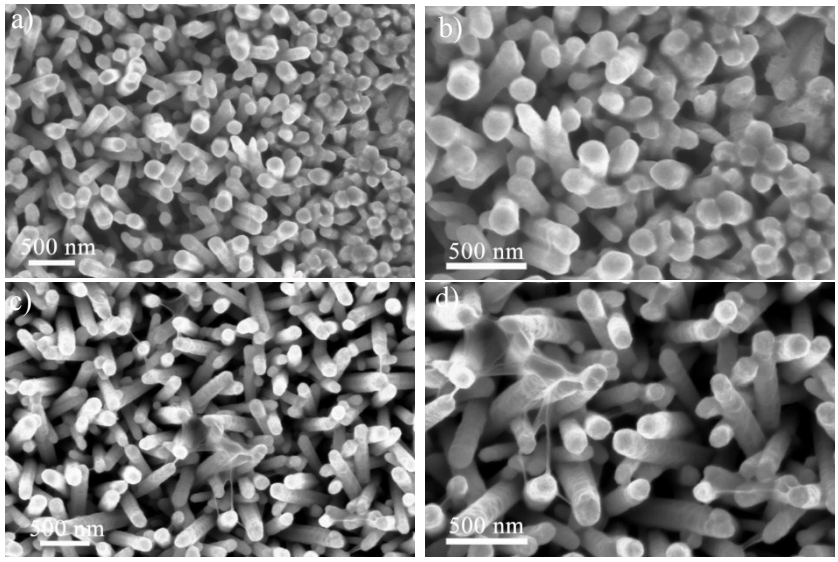

Fig. S14 SEM images of a, b) ZnO and c, d) Ni-Bi/rGO/ZnO after potentiostatic measurements.

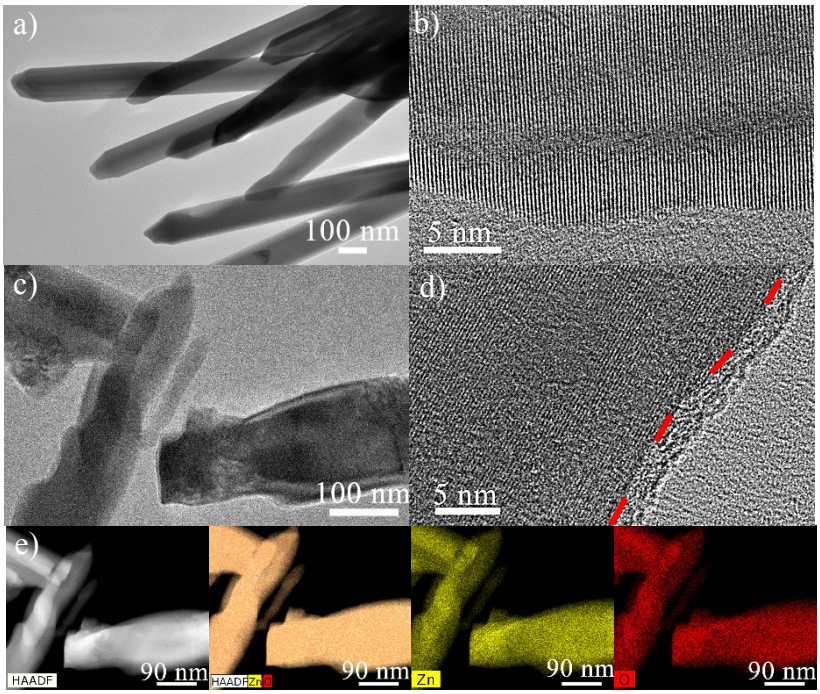

Fig. S15 a) TEM and b) HRTEM images of pristine ZnO. c) TEM, d) HRTEM and e) HAADF-STEM with corresponding EDS mapping images of ZnO after the potentiostatic measurement.

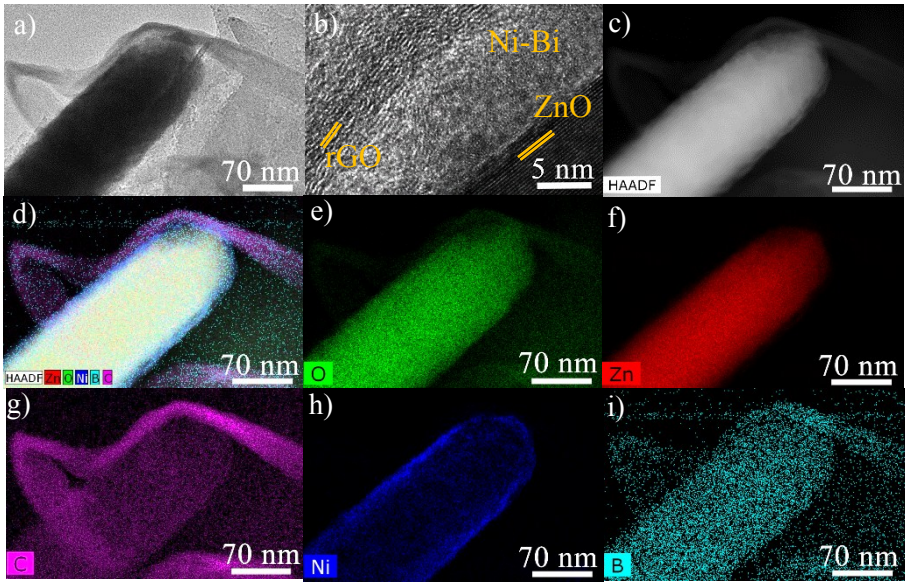

Fig. S16 a) TEM, b) HRTEM, c) HAADF-STEM, and d-i) EDS mapping images of Ni-Bi/rGO/ZnO after the potentiostatic measurement.

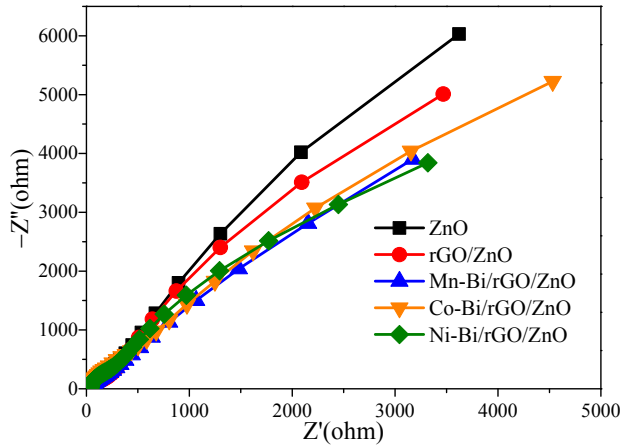

Fig. S17 Electrochemical impedance spectra (EIS) measured in dark.

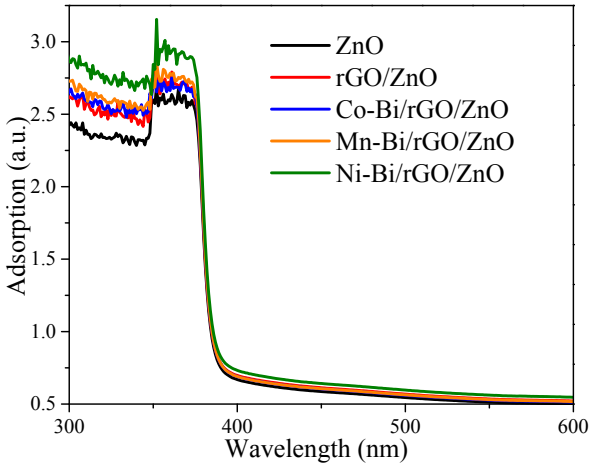

Fig. S18 UV-vis diffuse reflectance spectra of ZnO, rGO/ZnO and M-Bi/rGO/ZnO.

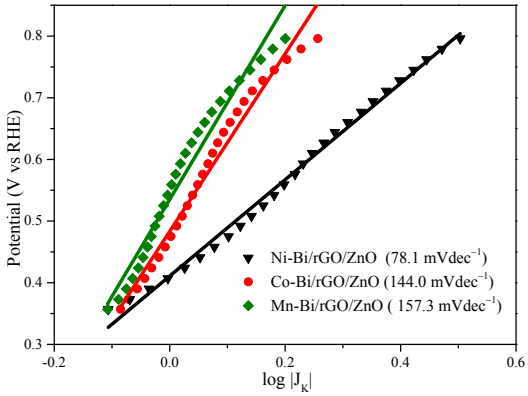

Fig. S19 Tafel plots for M-Bi/rGO/ZnO.

REFERENCES

1 G. Kresse and D. Joubert, *Phys. Rev. B*, 1999, **59**, 1758–1775.

2 P. E. Blöchl, *Phys. Rev. B*, 1994, **50**, 17953–17979.
3 G. Kresse and J. Furthmüller, *Comput. Mater. Sci.*, 1996, **6**, 15–50.
4 G. Kresse and J. Furthmüller, *Phys. Rev. B*, 1996, **54**, 11169–11186.
5 G. Kresse and J. Hafner, *Phys. Rev. B*, 1993, **48**, 13115–13118.
6 J. P. Perdew, K. Burke and M. Ernzerhof, *Phys. Rev. Lett.*, 1996, **77**, 3865–3868.
7 Y. Li, Y.-L. Li, B. Sa and R. Ahuja, *Catal. Sci. Technol.*, 2017, **7**, 545–559.
8 S. Dudarev and G. Botton, *Phys. Rev. B - Condens. Matter Mater. Phys.*, 1998, **57**, 1505–1509.
9 C. Ling, L. Q. Zhou and H. Jia, *RSC Adv.*, 2014, **4**, 24692–24697.
10 D. A. Tompsett, D. S. Middlemiss and M. S. Islam, *Phys. Rev. B - Condens. Matter Mater. Phys.*, 2012, **86**, 1–8.
11 H. Zhang, W. Tian, Y. Li, H. Sun, M. O. Tade and S. Wang, *J. Mater. Chem. A*, 2018, **6**, 6265–6272.
12 C. Gandolfi, T. Cotting, P. N. Martinho, O. Sereda, A. Neels, G. G. Morgan and M. Albrecht, *Dalt. Trans.*, 2011, **40**, 1855–1865.
13 R. S. Khnayzer, M. W. Mara, J. Huang, M. L. Shelby, L. X. Chen and F. N. Castellano, *ACS Catal.*, 2012, **2**, 2150–2160.
14 D. A. Links, *Nanoscale*, 2012, **4**, 6515–6519.
15 A. Sheikh, A. Yengantiwar, M. Deo and S. Kelkar, *Small*, 2013, **9**, 2091–2096.
16 Z. Li, S. Feng, S. Liu, X. Li, L. Wang and W. Lu, *Nanoscale*, 2015, **7**, 19178–19183.
17 Y. Mao, H. Yang, J. Chen and J. Chen, *Nano Energy*, 2014, **6**, 10–18.
18 J. Gong, *Nanoscale*, 2014, **7**, 77–81.
19 J. Li, H. Cheng, Y. Chiu and Y. Hsu, *Nanoscale*, 2016, **8**, 15720–15729.
20 Z. Zeng, F. Xiao, X. Gui, R. Wang, T. Thatt and Y. Tan, *J. Mater. Chem. A*, 2016, **4**, 16383–16393.
21 K. Zhao, X. Yan, Y. Gu, Z. Kang, Z. Bai, S. Cao, Y. Liu, X. Zhang and Y. Zhang, *Small*, 2016, **12**, 245–251.
22 V. A. Online, *Nanoscale*, 2014, **6**, 8769–8780.
23 C. E. T. Al, *ACS Nano*, 2012, **6**, 7362–7372.
24 D. Shao, Y. Cheng, J. He, D. Feng, L. Zheng, L. Zheng, X. Zhang, J. Xu, W. Wang, W. Wang, F. Lu, H. Dong, L. Li, H. Liu, R. Zheng and H. Liu, *ACS Catal.*, 2017, **7**, 5308–5315.